Allosteric Neutralization by Human H7N9 Antibodies

Xueling Wu (xw2702@cumc.columbia.edu)
Columbia University https://orcid.org/0000-0002-9752-3734

Manxue Jia
Aaron Diamond AIDS Research Center

HanJun Zhao
The University of Hong Kong https://orcid.org/0009-0001-9014-6972

Nicholas Morano
Department of Biochemistry, Zuckerman Mind Brain Behavior Institute, Columbia University

Hong Lu
Aaron Diamond AIDS Research Center, Columbia University Vagelos College of Physicians and Surgeons

Yin-Ming Lui
State Key Laboratory for Emerging Infectious Diseases, Carol Yu Centre for Infection, Department of Microbiology, School of Clinical Medicine, Li Ka Shing Faculty of Medicine, University of Hong Kon

Haijuan Du
Vaccine Research Center, National Institute of Allergy and Infectious Diseases, National Institutes of Health

Jordan Becker
Department of Biochemistry, Zuckerman Mind Brain Behavior Institute, Columbia University

Kwok-Yung Yuen
The University of Hong Kong https://orcid.org/0000-0002-2083-1552

David Ho
Columbia University Irving Medical Center https://orcid.org/0000-0003-1627-149X

Peter Kwong
Vaccine Research Center, National Institute of Allergy and Infectious Diseases https://orcid.org/0000-0003-3560-232X

Lawrence Shapiro
Department of Biochemistry, Zuckerman Mind Brain Behavior Institute, Columbia University

Kelvin Kai-Wang To
The University of Hong Kong https://orcid.org/0000-0002-1921-5824

Article

Keywords:

Posted Date: November 7th, 2023

DOI: https://doi.org/10.21203/rs.3.rs-3429355/v1

Additional Declarations: Yes there is potential Competing Interest. An U.S. provisional patent titled “Human Protective Neutralizing and Non-neutralizing Antibodies and Their Use against Influenza Viruses” was filed with filing No. 63/578,505 and XW, MJ, NCM, HL, DDH, KY, KKT, PDK, and LS as co-inventors.

Allosteric Neutralization by Human H7N9 Antibodies

Manxue Jia[1†], Hanjun Zhao[2,3†], Nicholas C. Morano[4,5†], Hong Lu[1,5], Yin-Ming Lui[2], Haijuan Du[6], Jordan E. Becker[4,5], Kwok-Yung Yuen[2,3,7], David D. Ho[1,5], Peter D. Kwong[4,6], Lawrence Shapiro[4,5], Kelvin Kai-Wang To[2,3,7]*, Xueling Wu[1,5]*

[1]Aaron Diamond AIDS Research Center, Affiliate of Rockefeller University, New York, NY 10016, USA.

[2]State Key Laboratory for Emerging Infectious Diseases, Carol Yu Centre for Infection, Department of Microbiology, School of Clinical Medicine, Li Ka Shing Faculty of Medicine, University of Hong Kong, Pokfulam, Hong Kong Special Administrative Region, China.

[3]Centre for Virology, Vaccinology and Therapeutics, Hong Kong Science and Technology Park, Sha Tin, Hong Kong Special Administrative Region, China.

[4]Department of Biochemistry, Zuckerman Mind Brain Behavior Institute, Columbia University, New York, NY 10027, USA.

[5]Aaron Diamond AIDS Research Center, Columbia University Vagelos College of Physicians and Surgeons, New York, NY 10032, USA.

[6]Vaccine Research Center, National Institute of Allergy and Infectious Diseases, National Institutes of Health, Bethesda, MD 20892, USA.

[7]Department of Clinical Microbiology and Infection, University of Hong Kong-Shenzhen Hospital, Shenzhen, Guangdong, China.

[†]These authors contributed equally to this work.

*Correspondence to: Xueling Wu (email: xw2702@cumc.columbia.edu)

Kelvin Kai-Wang To (email: kelvinto@hku.hk)

Abstract: The avian influenza A virus H7N9 causes severe human infections with more than 30% fatality despite the use of neuraminidase inhibitors. Currently there is no H7N9-specific prevention or treatment for humans. From a 2013 H7N9 convalescent case occurred in Hong Kong, we isolated four H7 hemagglutinin (HA)-reactive monoclonal antibodies (mAbs) by single B cell cloning, with three mAbs directed to the HA globular head domain (HA1) and one to the HA stem region (HA2). Two clonally related HA1-directed mAbs, H7.HK1 and H7.HK2, potently neutralized H7N9 and protected mice from a lethal H7N9/AH1 challenge. Cryo-EM structures revealed that H7.HK1 and H7.HK2 bind to a β14-centered surface partially overlapping with the antigenic site D of HA1 and disrupt the 220-loop that makes hydrophobic contacts with sialic acid on the adjacent protomer, thus affectively blocking viral entry. The more potent mAb H7.HK2 retained full HA1 binding and neutralization capacity to later H7N9 isolates from 2016-2017, which is consistent with structural data showing that the antigenic mutations of 2016-2017 from the 2013 H7N9 only occurred at the periphery of the mAb epitope. The HA2-directed mAb H7.HK4 lacked neutralizing activity but protected mice from the lethal H7N9/AH1 challenge when engineered to mouse IgG2a enabling Fc effector function in mice. Used in combination with H7.HK2 at a suboptimal dose, H7.HK4 augmented mouse protection. Our data demonstrated an allosteric mechanism of mAb neutralization and augmented protection against H7N9 when a HA1-directed neutralizing mAb and a HA2-directed non-neutralizing mAb were combined.

INTRODUCTION

H7N9 is an avian influenza A group 2 virus first transmitted to humans in the spring of 2013 most likely through live poultry market exposure in China (*1-3*). The virus reemerged in the fall of 2013 and in the winter of later years, with the largest epidemic reported as the 5th wave in 2016-2017 (*4-6*). Though there is limited evidence for human-to-human transmission, few mutations in the hemagglutinin (HA) gene of the virus might be sufficient to overcome its inefficiency for human transmission (*7-10*). Like other influenza virus infections, the most common treatment against H7N9 is the neuraminidase inhibitor oseltamivir, but oseltamivir-resistant strains have emerged (*11-13*). Intravenous (i.v.) zanamivir, though not clinically approved, has been used on a compassionate basis in some severe cases because of favorable pharmacokinetics and *in vitro* susceptibility against oseltamivir-resistant strains (*14, 15*); however, the effectiveness of i.v. zanamivir against H7N9 has not been validated in large clinical trials. Despite the use of neuraminidase inhibitors, H7N9 case-fatality rate remains higher than 30%, and currently there is no licensed vaccine against H7N9 for humans. An endonuclease inhibitor baloxavir marboxil, targeting the virus polymerase acid, protected mice from lethal H7N9 challenge (*16*), but treatment for human H7N9 infection with this inhibitor has not been reported. Concerns for a major outbreak and lack of effective treatment warrant further studies to identify and develop human monoclonal antibodies (mAbs) with potent antiviral functions against H7N9.

Because HA is the major target for influenza neutralizing antibodies, H7-reactive human mAbs have been isolated and characterized from H7N9 acute infections (*17*), convalescent cases (*18*), and H7N9 experimental vaccinees (*19-21*). The binding sites of these mAbs have been mapped to the HA globular head (HA1) and stem (HA2) domains. A subset of HA1-directed mAbs

potently neutralized H7N9 and protected mice from H7N9 challenges at doses of 0.3, 1, 5 mg/kg or higher (*17-20*). These HA1-directed mAbs typically neutralized H7N9 by direct interference with or around the receptor (sialic acid) binding site (*17, 19, 22*). These epitopes correspond to the antigenic sites of A and B as previously mapped on the surface of H3 HA (*23-25*). Of note, significant antigenic drift has been documented in the HA gene of 2016-2017 H7N9 from the initial 2013 isolates (*17, 26, 27*). For example, Huang *et al* isolated 17 neutralizing mAbs from four cases infected in 2013 and 2014, yet only three of these mAbs were active against viral isolates from 2016-2017 (*17*). A broad mAb FluA-20 targeting the HA1 trimer interface did not mediate neutralization *in vitro*, but protected mice from viral challenges by disrupting HA trimers and inhibiting cell-to-cell spread of virus (*21*). HA2-directed mAbs typically lacked neutralizing activity, yet a few of them protected mice from H7N9 challenges at 5 mg/kg (*20*), especially when the mAbs were engineered as mouse IgG2a that has the highest Fc-mediated effector functions in mouse (*28*). These studies have not tested the combination of two or more mAbs that target different regions of H7N9 HA.

In the post COVID-19 era, preparedness for future pandemics has risen with high enthusiasm. We aim to facilitate the development of human mAbs against H7N9, which has been considered one of the most serious pandemic threats. We have obtained peripheral blood mononuclear cells (PBMCs) from a 2013 H7N9 convalescent case in Hong Kong with the virus isolated as A/Hong Kong/470129/2013 H7N9 (*14*). The course of this infection lasted for about one month and the treatment required extracorporeal membrane oxygenation (ECMO) and i.v. zanamivir (*14*). Development of plasma neutralizing antibodies was evident at recovery. The PBMC sample we used to isolate mAbs was collected one year post recovery.

RESULTS

H7-reactive mAb isolation

For H7-specific mAb isolation, we purchased a soluble recombinant H7 HA protein based on A/Shanghai2/2013 H7N9 for biotinylation, followed by streptavidin-PE conjugation. With this H7-PE bait, we stained 5 million PBMCs from the H7N9_HK2013 donor and sorted a total of 68 IgG^+ B cells (defined as $CD3^-CD19^+CD20^+IgG^+$) that are H7-PE^+ (**Fig. 1A**). Most of the sorted cells were at the borderline of H7-PE staining, but a few stained brightly for H7-PE. From the sorted B cells, we performed single B cell RT-PCR and recovered four H7-reactive mAbs – namely, H7.HK1, H7.HK2, H7.HK3, and H7.HK4.

Measured by ELISA, the four reconstituted mAbs bound tightly to the H7N9 HA antigen used for H7-PE staining and to a recombinant H7N7 HA antigen based on A/Netherlands/219/2003 H7N7 (**Fig. 1B**, upper panels). Pre-treating the H7N9 HA with Endoglycosidase H (Endo H) had no effect on the mAb binding profiles, indicating that these mAbs do not rely on H7 glycans for binding (**Fig. 1B**, upper panels). After switching the ELISA coating antigen to HA1 of the matching H7N9 HA from A/Shanghai2/2013, the binding curves of H7.HK1, H7.HK2, and H7.HK3 were fully retained, indicating that these mAbs bind to the globular head domain HA1; in contrast, H7.HK4 lost binding to H7N9 HA1, indicating that its binding epitope is likely located in the HA2 stem domain (**Fig. 1B**, middle panels). Because of the documented antigenic drift for 2016-2017 H7N9 isolates, we also tested the mAb binding to HA1s from A/Guangdong/17SF003/2016 H7N9 and A/Hong Kong/125/2017 H7N9. The binding curves of H7.HK1, H7.HK2, and H7.HK3 to both 2016 and 2017 HA1s were fully retained, and H7.HK4 did not bind to any HA1s (**Fig. 1B**, middle panels). Additionally, we tested these mAbs for binding to 6 other non-H7 HA proteins. Though H7.HK1 and H7.HK2 did not react with any non-H7 HA,

H7.HK3 cross-reacted with H15N8 HA, and H7.HK4 cross-reacted with H10N8 and H15N8 HAs (**Fig. 1B**, lower panels), which sequence-wise are the closest to H7 in group 2 influenza HA genes (*29*).

H7-reactive mAb neutralization

Using expression plasmids separately encoding H7 and N9 genes from A/Shanghai/4664T/2013 to pseudotype with HIV-1 NL4-3-lucΔ*env* backbone (*30*), we generated the H7N9 2013 pseudotype particles and tested mAb neutralization by a luciferase readout from single round infection of MDCK cells (**Fig. 1C, left**). H7.HK1 and H7.HK2 each potently neutralized the H7N9 2013 pseudovirus with IC_{50}s of 5 and 2 ng/mL respectively, while the other two mAbs H7.HK3 and H7.HK4 did not neutralize at up to 10 μg/mL (**Fig. 1C, left, Table 1**). Similarly, we generated pseudovirus using an expression plasmid encoding H7 from A/Guangdong/17SF003/2016 H7N9. H7.HK2 fully retained its potent neutralization against the H7N9 2016 pseudovirus with an IC_{50} of 2 ng/mL, and H7.HK1's neutralization was reduced to an IC_{50} of 16 ng/mL, while the other two mAbs H7.HK3 and H7.HK4 did not neutralize (**Fig. 1C, right, Table 1**). We further assessed the mAb neutralization against three live replicating H7N9 viruses, Anhui1 (AH1), Zhejiang (ZJ), and the donor's autologous isolate A/Hong Kong/470129/2013, for multiple rounds of infection in MDCK cells. Scored by the presence of cytopathic effect, mAbs H7.HK1 and H7.HK2 neutralized all three H7N9 live isolates with IC_{50}s ranging 0.3-1 μg/mL; however, they did not neutralize any non-H7N9 influenza isolates tested, indicating that these mAbs are specific to H7N9 (**Table 1**). The other two mAbs H7.HK3 and H7.HK4 did not neutralize any of the tested H7N9 and therefore were not tested against non-H7N9 viruses. The neutralization IC_{50}s of H7.HK1 and H7.HK2 using the pseudovirus were about 100-fold more potent than those using the live replicating viruses, suggesting that the pseudovirus neutralization

is more sensitive thus useful for initial screening of neutralizing mAbs, which could then be confirmed with live replicating viruses. Similar differences in IC_{50} values have been reported for other HA-reactive mAbs tested by both pseudovirus and live replicating virus (*31*).

Table 1 Neutralization IC_{50} of H7.HK mAbs against pseudovirus or live replicating virus

mAb ID	Neutralization IC_{50} (μg/mL) in MDCK cells									
	H7N9 2013 pseudovirus	H7N9 2016 pseudovirus	H7N9/ AH1	H7N9/ ZJ	H7N9/HK 470129	H3N2/ 400500	H1N1/ 415742	H5N1/ 459094	H5N1/ 1194	H9N2/ 1073
H7.HK1	0.005	0.016	0.3	0.3	0.4	>30	>30	>30	>30	>30
H7.HK2	0.002	0.002	0.3	1.0	0.9	>30	>30	>30	>30	>30
H7.HK3	>10	>10	>30	>30	ND	ND	ND	ND	ND	ND
H7.HK4	>10	>10	>30	>30	ND	ND	ND	ND	ND	ND

"ND" indicates "not done".

H7-reactive mAb sequences

Sequence analysis revealed that all four H7.HK mAbs are IgG1 (**Table 2**). H7.HK1 and H7.HK2 are clonal variants using IGHV4-59 for heavy chain with 8-10% somatic hypermutation (SHM) and a complementarity-determining region (CDR) H3 of 11 amino acids according to the Chothia definition (*32-34*), and IGKV2-28 for light chain with 6% SHM and a CDR L3 of 9 amino acids. Though clonally related, H7.HK1 and H7.HK2 share only 3 out of 13-15 amino acid SHMs in the heavy chain V-gene and 1 out of 8 amino acid SHMs in the light chain V-gene (**Supplementary Fig. 1**). A putative N-linked glycosylation site is present in the light chain CDR L1 of H7.HK1 and H7.HK2. H7.HK3 uses IGHV7-4-1 for heavy chain with 7% SHM and a CDR H3 of 14 amino acids, and IGKV1-5 for light chain with 5% SHM and a CDR L3 of 8 amino acids. A putative N-linked glycosylation site is also present in H7.HK3 at the heavy chain CDR H2. H7.HK4 uses IGHV4-61 for heavy chain with 7% SHM and a CDR H3 of 13 amino acids, and IGKV1-16 for light chain with 5% SHM and a CDR L3 of 9 amino acids (**Table 2**, **Supplementary Fig. 1**).

Table 2 Genetic composition, epitope, and neutralization function of H7.HK mAbs

mAb ID	Origin	Time point	Isotype	V-gene (SHM%)	CDR3 length in amino acid	Epitope	Neutralization
H7.HK1	Human	1 year post recovery	IgG1	HV4-59 (8%) KV2-28 (6%)	H3: 11, L3: 9	H7 HA1	Yes
H7.HK2	Human	1 year post recovery	IgG1	HV4-59 (10%) KV2-28 (6%)	H3: 11, L3: 9	H7 HA1	Yes
H7.HK3	Human	1 year post recovery	IgG1	HV7-4-1 (5%) KV1-5 (7%)	H3: 14, L3: 8	H7 HA1	No
H7.HK4	Human	1 year post recovery	IgG1	HV4-61 (7%) KV1-16 (5%)	H3: 13, L3: 9	H7 HA2	No

H7-reactive mAb structures

For structural analysis, we generated the antibody fragments for antigen binding (Fabs) and expressed the H7 HA trimer by transient transfection of Expi293F cells. We froze grids containing the Fab:HA complexes and determined cryo-EM structures of each Fab bound to an H7 HA trimer. A resolution of 3.62 Å for H7.HK1 and 3.69 Å for H7.HK2 was achieved (**Fig. 2A, Supplementary Fig. 2, Table S1**). These complex structures demonstrate that H7.HK1 and H7.HK2 are highly superimposable (**Fig. 2B**) and their interactions with H7 are centered at β14 and extended to the surfaces of β10 and β19 (**Fig. 2C**). This β14-targeting surface partially overlaps with the antigenic site D towards sites A and B as previously mapped on H3 (*23, 25*). Analysis of the H7.HK1 epitope demonstrates that most interactions are driven by the heavy chain and consist of seven hydrogen bonds (Y52:E111, R97:G114, G102:S158, D103:T116, Y104:T156, Y104:S158, S106:T116) and one salt bridge (H53:E111) (**Fig. 2D**). The light chain is less involved in binding, making only one hydrogen bond (Y54:Q154) and weak hydrophobic interactions (**Fig. 2E**). The light chain of both H7.HK1 and H7.HK2 are glycosylated in CDR L1; this glycan plays no role in binding, but there is good density to support its presence. The epitope of H7.HK2 is similar to that of H7.HK1, only differing in slight contacts on the periphery (**Supplementary Fig. 3A**). Additionally, nearly all hydrogen bonds are conserved

between the two antibodies (**Supplementary Fig. 3B**). However, the substitution of F61S in CDR L2 of H7.HK2 results in an additional hydrogen bond with HA G119. This substitution also shifts the orientation of H7.HK2 CDR L2 slightly so that Y54 interacts with T156 for H7.HK2 instead of Q154 for H7.HK1 (**Supplementary Fig. 3C**). Finally, as H53 is substituted with tyrosine in the heavy chain of H7.HK2, it does not make the H53:E111 salt bridge.

To analyze the mechanism of neutralization, we first compared the binding site of H7.HK1 to that of four other H7-reactive antibodies with published structures, L4A-14, L4B-18, L3A-44 (PDB: 6II4, 6II8, 6II9) (*17*) and H7.167 (PDB: 5V2A) (*19*). This analysis demonstrates that the binding site of H7.HK1 is almost completely distinct from that of these previously published antibodies, which compete for the receptor binding site (RBS) (**Fig. 2F**). The binding site of H7.HK1 is also distant from that of 07-5F01, which was mapped to an escape mutation R65K (corresponding to R47K here) of HA1 (*20*) (**Fig. 2F**). Strikingly, the epitope of H7.HK1 (β14-centered) is extremely distal to the RBS of the protomer it interacts with and is closer to the RBS on the adjacent protomer. To further examine the relationship between the mAb binding site and RBS, the human receptor analogue Sialylneolacto-N-tetraose c (LSTc) was modeled into the RBS of H7 (PDB: 4BSE) (*35*) in the H7.HK1 complex. Interestingly, there were no steric clashes between H7.HK1 and sialic acid bound to the adjacent protomer, and no mAb interaction with RBS (**Fig. 2G**). However, the HA 220-loop (G209-G219) that makes hydrophobic contacts with sialic acid has no density present in the structure of H7.HK1 or H7.HK2 bound to HA, suggesting that these antibody binding causes 220-loop to become disordered. All previously examined H7 structures, as well as an additional cryo-EM structure in which Fab 1D12 is bound to the stem region of H7 HA (PDB: 6WXL) (*36*) have consistent electron density accounting for

this loop. Alignments of the H7.HK1 complex structure with the crystal structure of H7 HA bound to LSTc (PDB: 4BSE) (*35*) demonstrate where the 220-loop would be when receptor is bound and that the light chain of H7.HK1 would clash with this loop (**Fig. 2H**), further supporting that H7.HK1 and H7.HK2 act by causing 220-loop to become disordered, thus preventing its interactions with the sialic acid receptor. The HA1 trimer interface mAb FluA-20 interacts with the non-RBS side of 220-loop on the protomer it interacts with (*21*). To our knowledge, the allosteric mechanism of neutralization employed by H7.HK1 and H7.HK2 is distinct from previously reported HA1-directed H7N9 neutralizing mAbs, which all directly compete with sialic acid for binding to HA on the protomer they interact with (*17, 19, 21, 22, 37*).

Since the H7N9 HA gene has significantly evolved and changed in 2016-2017 compared to that of 2013 (with up to 13 amino acid substitutions in HA1), we examined the locations of mutated residues in the epitopes of H7.HK1 and H7.HK2 that consist of 32 contacting residues in HA1 for both mAbs (**Supplementary Fig. 4A**). There are four mutations in the binding site of H7.HK1 and H7.HK2 – namely, A112T/P, S118N, G119E, and R163K, appeared in 2016-2017 compared to the 2013 H7N9, and all four mutations are located at one side edge of the epitopes (**Supplementary Fig. 4B**), thus not altering the mAb interactions with HA1. This analysis is in consistency with the intact binding of H7.HK1 and H7.HK2 to both 2016 and 2017 HA1s aligned to the 2013 HA1 (**Fig. 1B**, middle panels) and H7.HK2's full retention of neutralization against the H7N9 2016 pseudovirus (**Fig. 1C**).

H7-reactive mAb mouse protection

We next assessed the prophylactic and therapeutic effect of H7.HK mAbs as human IgG1 in a mouse lethal challenge model. To assess mAb prophylactic effect, balb/c mice (n = 5-10 per group from 1-2 experiments) were injected intraperitoneally (i.p.) with human H7N9 mAbs one day before intranasal (i.n.) challenge of 10-fold 50% lethal dose (10 LD_{50}) of A/Anhui/1/2013 H7N9 virus. Given 100 μg per mouse (equivalent to 5 mg/kg), the neutralizing mAbs H7.HK1 and H7.HK2 each fully protected mice without apparent weight loss (**Fig. 3A**, top panels); given 20 μg per mouse (equivalent to 1 mg/kg), H7.HK2 still fully protected mice from death (defined as ≥ 20% weight loss), with up to 8% average weight loss; H7.HK1 protected 7 out of 10 mice from death, with up to 12% average weight loss for mice that survived (**Fig. 3A**, upper middle panels). By day 2 post challenge, the weight preservation was significantly better in mice receiving 20 μg of H7.HK1 or H7.HK2 than mice receiving the placebo mAb or phosphate buffered saline (PBS). Mice receiving the non-neutralizing mAbs H7.HK3 or H7.HK4 (100 μg or 20 μg) were not protected and showed no difference from placebo mAb and PBS controls (**Fig. 3A**, top and upper middle panels).

Since anti-HA2 stem mAbs have demonstrated Fc-mediated protection against influenza (*38*), we converted the anti-HA2 non-neutralizing mAb H7.HK4 to mouse IgG2a (mIgG2a) – an isotype that mediates strong Fc effector function in mice, and tested it for prophylaxis in the mouse challenge model, along with mouse IgG1 (mIgG1), which lacks Fc effector function in mice (*28*). Given 100 μg per mouse, H7.HK4 mIgG2a but not mIgG1 protected 4 out of 5 mice from death, with up to 17% average weight loss for mice that survived (**Fig. 3A**, lower middle panels). By day 3 post challenge, the weight preservation was significantly better in mice receiving

H7.HK4 mIgG2a than mice receiving H7.HK4 mIgG1 or placebo mIgG2a. Though survived, mice receiving 100 μg H7.HK4 mIgG2a lost more weight than those receiving 20 μg neutralizing mAbs H7.HK1 or H7.HK2 (**Fig. 3A**, upper middle panels), indicating less prophylaxis efficiency for H7.HK4 (as mIgG2a) than H7.HK1 and H7.HK2.

Since the H7.HK2 and H7.HK4 mAbs bind to different sites on the HA and protect through different mechanisms, we tested the combination of suboptimal dose of 20 μg H7.HK2 (as human IgG1) with 100 μg H7.HK4 mIgG2a in the mouse challenge model, using 20 μg H7.HK2 (as human IgG1) with 100 μg H7.HK4 mIgG1 as a control. Compared to this control group, which protected 9 out of 10 mice from death and lost up to 11% body weight for mice that survived, the combination of 20 μg of H7.HK2 (as human IgG1) with 100 μg H7.HK4 mIgG2a fully protected mice from death, with only up to 7% weight loss, and the weight difference was statistically significant between these two groups since day 3 post challenge (**Fig. 3A**, bottom panels), indicating a beneficial role of H7.HK4 in the mAb combination regimen.

To assess mAb therapeutic effects, we first i.n. challenged mice (n = 5-10 per group from 1-2 experiments) with 10 LD_{50} of A/Anhui/1/2013 H7N9 virus, waited for one day, and then on day 1 post challenge i.p. injected mice with 100 μg H7.HK1 or H7.HK2 as human IgG1, or H7.HK4 as mIgG2a (**Fig. 3B**). Twelve and 13 out of 15 mice receiving 100 μg H7.HK1 or H7.HK2 one day after viral challenge initially lost weight similarly to placebo and PBS controls but then started to recover on day 5 after challenge. Therefore, the neutralizing mAbs H7.HK1 and H7.HK2 showed both prophylactic and therapeutic efficacies in the mouse lethal challenge model. None of the 5 mice receiving 100 μg H7.HK4 mIgG2a one day after challenge survived

(**Fig. 3B**), indicating that H7.HK4 as mIgG2a demonstrated measurable prophylactic effect but not therapeutic efficacy.

DISCUSSION

Already endemic, adapted, and evolved in humans for 10 years, H7N9 continues to post risk and infect human cases exposed to infected poultry in China. While the current risk to public health is low, the pandemic potential of H7N9 is especially concerning if it were to gain the ability of sustained human-to-human transmission. Based on its biological features such as dual affinity for avian and human receptors, high case-fatality rate, resistance to neuraminidase inhibitors, and lack of pre-existing immunity in the human populations, there is an immediate need and interest to develop human mAb prophylaxis and therapeutics against H7N9, to which a specific treatment or licensed vaccine (for humans) is not available.

In this study, we identified two HA1-directed clonally related human mAbs, H7.HK1 and H7.HK2, that neutralized H7N9 with potencies and mouse protection efficacies (prophylactic and therapeutic) in line with the best of previously reported H7N9 mAbs. Specifically, a combined phage library from three H7N9 convalescent cases yielded a single neutralizing mAb clone (*18*). Despite possible nonnative heavy and light chain pairing from phage display, the best member of the mAb clone, HNIgGA6, neutralized H7N9 and protected mice against a lethal challenge at 5 mg/kg with up to about 10% weight loss (*18*). Likewise, from a study of four H7N9 acutely infected cases, the best mAb L4A-14 cloned from plasmablast protected mice against a lethal challenge at 10 mg/kg with up to about 10% weight loss (*17*). The most potent mAb H7.167 from a study of EBV transformed B cells from five representative H7N9

experimental vaccinees neutralized H7N9 and protected mice against a sub-lethal challenge of H7-PR8 at 1.65 mg/kg without apparent weight loss (*19*). The best HA1-directed neutralizing mAb 07-5F01 from a study of H7N9 experimental vaccinees' plasmablasts protected mice against a lethal challenge at 0.3 mg/kg without apparent weight loss (*20*). The broad HA1 trimer interface mAb FluA-20 from a healthy donor with extensive influenza vaccinations lacked *in vitro* neutralization but protected mice against a sub-lethal challenge of H7-PR8 at 10 mg/kg without apparent weight loss (*21*). In comparison, H7.HK1 and H7.HK2 protected mice against a lethal challenge at 1 mg/kg with up to 12% weight loss.

We have also structurally defined the epitopes of H7.HK1 and H7.HK2 to the β14-centered surface of H7 HA1, partially overlapping with the antigenic site D rather than the commonly targeted RBS and trimer interface by previous H7N9 mAbs (*37*), including the best reported human mAbs discussed above. Structural alignments and comparisons demonstrated that H7.HK1 and H7.HK2 interacted with H7 completely differently from L4A-14, H7.167, 07-5F01, and FluA-20. By escape mutations, a previous H3 neutralizing mAb D1-8 was mapped to the lower part of antigenic site D towards site E (*39*); this epitope partially overlaps with the H7.HK1 and H7.HK2 epitope described here. However, without structural data, the action of neutralization by D1-8 cannot be determined. Importantly, D1-8 does not react to H7, and likewise, H7.HK1 and H7.HK2 do not react to H3. Hence, D1-8 cannot replace the anti-H7N9 function of H7.HK1 and H7.HK2. The unique β14-targeting epitope on HA1 would render H7.HK1 and H7.HK2 favorable candidates for combination prophylaxis and therapy against H7N9 to augment protection efficacy and increase the genetic barrier for viral escape.

H7N9 has evolved over time and its HA gene has significantly changed in 2016-2017 compared to that of 2013. Consequently, most neutralizing mAbs isolated from individuals infected or vaccinated with the 2013 H7 HA lost reactivity to 2016-2017 isolates, requiring updated H7 immunogens for mAb and vaccine development (*17*). We show that four mutations appeared in 2016-2017 are located at the periphery of the H7.HK1 and H7.HK2 epitopes and confirmed that the binding profiles of H7.HK1 and H7.HK2 are intact to both 2016 and 2017 HA1s as compared to 2013 HA1. We also showed that H7.HK2 fully retained its potent neutralization (IC_{50} of 2 ng/mL) against the H7N9 2016 pseudovirus, while H7.HK1's neutralization IC_{50} was weakened from 5 to 16 ng/mL. Previous protective mAbs such as HNIgGA6 (*18*), H7.167 (*19*), and 07-5F01 (*20*) were not evaluated for reactivity to H7N9 2016-2017 isolates. L4A-14 was active against A/Guangdong/TH005/2017 (an avian virus related to A/Guangdong/17SF003/2016) but required 10 mg/kg, compared to 1 mg/kg of H7.HK1 and H7.HK2, for mice protection with up to about 10% weight loss (*17*). Compared to a 2013 H7N9 isolate, the neutralization IC_{50} of 07-5F01 was reduced by more than 100-fold against A/mallard/Netherlands/12/2000 H7N7 (*20*), and H7.167 did not recognize H7 from A/Netherlands/219/2003 H7N7 (*19*), to which all four H7.HK mAbs from the present study bound tightly.

Lastly, we tested a suboptimal dose of H7.HK2 combining with the HA2-directed non-neutralizing mAb H7.HK4 against mouse lethal challenge. Compared to HA1 (head region of HA), HA2 (stem region) is genetically more conserved. Hence, HA2-directed mAbs typically display broader recognition of HA subtypes than HA1-directed mAbs. This is indeed the case for H7.HK4, i.e., in addition to H7N9 and H7N7, it also recognized the HAs from H10N8 and H15N8, to which both H7.HK1 and H7.HK2 had no reactivity. When converted to mouse IgG2a

enabling Fc effector function in mice, H7.HK4 demonstrated measurable prophylactic protection at 5 mg/kg and augmented mouse protection of H7.HK2, supporting the inclusion of HA2-directed antibodies in a mAb combination regimen against H7N9.

In summary, from a 2013 H7N9 convalescent case occurred in Hong Kong, we isolated two clonally related HA1-directed neutralizing mAbs, H7.HK1 and H7.HK2, that demonstrated prophylactic and therapeutic efficacies in a mouse lethal challenge model. Cryo-EM structures revealed a β14-centered site of vulnerability targeted by H7.HK1 and H7.HK2, which allowed full binding and neutralization capacity of H7.HK2 to the later 2016-2017 H7N9 isolates. This unique epitope renders H7.HK2 a favorable candidate for combination prophylaxis and therapy against H7N9, which may include multiple HA1-directed neutralizing mAbs targeting different epitopes and benefit from the inclusion of HA2-directed mAbs as well.

METHODS

Collection of human specimens

A blood specimen was collected from the H7N9_HK2013 patient about one year after recovery from a hospitalized severe H7N9 infection. Written informed consent was obtained from the patient. The study was approved by the Institutional Review Board (IRB) of the University of Hong Kong and the Hospital Authority (Reference number: UW-13-265).

Plasmids, viruses, antibodies, and cells

Expression plasmids encoding the H7 hemagglutinin and N9 neuraminidase based on A/Shanghai/4664T/2013 H7N9 strain were obtained from Dr. Jianqing Xu (*30*). Codon-optimized gene encoding the H7 hemagglutinin of A/Guangdong/17SF003/2016 H7N9 was

synthesized (Twist Bioscience) and cloned into pcDNA3.1 (Invitrogen). HIV-1 pNL4-3.Luc.R-E- backbone was obtained through the NIH HIV Reagent Program, as contributed by Dr. Nathaniel Landau. These plasmids were used to co-transfect 293T cells (ATCC, Manassas, VA) to generate H7N9 2013 and 2016 pseudoviruses. All live replicating influenza A viruses used in this study were isolated from patients and include A/Hong Kong/470129/2013 H7N9 (*14*), A/Zhejiang/DTID-ZJU01/2013 H7N9 (*3*), A/Anhui/1/2013 H7N9 (obtained from the China Center for Disease Control and Prevention), A/Vietnam/1194/2004 H5N1, A/Hong Kong/ 459094/2010 H5N1, A/Hong Kong/1073/1999 H9N2, A/Hong Kong/415742/2009 H1N1, and A/Hong Kong/400500/2015 H3N2. The non-H7N9 placebo mAb used in this study, AD358_n1, has been described (*40*) and is specific to HIV-1 gp120. Human embryonic kidney 293 cell line, of which the sex is female, is the parental cell for 293T and Expi293F cell lines. 293T was obtained from ATCC and maintained as adherent cells in complete DMEM medium at 37ºC. 293T is highly transfectable and contains SV40 T-antigen. Expi293F was obtained from ThermoFisher and adapted to suspension culture in Expi293 Expression Medium at 37ºC. The Madin-Darby Canine Kidney (MDCK) cell line, of which the sex is female, was obtained from ATCC and maintained as adherent cells in complete DMEM medium at 37ºC.

Single B cell sorting by fluorescence activated cell sorter (FACS)

A soluble recombinant HA antigen based on A/Shanghai/2/2013 H7N9 (Immune Technologies, New York, NY) was biotinylated, followed by streptavidin mediated conjugation of phycoerythrin (PE) (Invitrogen). PBMCs were stained with an antibody cocktail to CD3-PE-CF594 (BD Biosciences, San Jose, CA), CD19-PE-Cy7 (BioLegend, San Diego, CA), CD20-APC-Cy7 (BioLegend), IgG-FITC (BD Biosciences), and IgM-V450 (BD Biosciences). In

addition, live/dead yellow stain (Invitrogen) was used to exclude dead cells. After washing, cells were sorted using a multi-laser MoFlo sorter (Beckman Coulter, Jersey City, NJ). Fluorescence compensation was performed with anti-mouse Ig kappa chain beads (BD Biosciences) stained with each antibody in a separate tube. Individual B cells were sorted into a 96-well PCR plate, each well containing 20 μL lysis buffer, composed of 0.5 μL RNaseOut (Invitrogen), 5 μL 5x first-strand buffer, 1.25 μL 0.1M DTT, and 0.0625 μL Igepal (Sigma, St. Louis, MO). The PCR plate with sorted cells was frozen on dry-ice and then stored at -80˚C. The total cell sample passing through the sorter was analyzed with FlowJo (TreeStar, Cupertino, CA).

Single B cell RT-PCR, sequencing, and cloning

From each sorted cell, the variable regions of IgG heavy and light chains were amplified by RT-PCR and cloned into expression vectors as previously described (*40*). Briefly, frozen plates with single B-cell RNA were thawed at room temperature, and RT was carried out by adding into each well 3 μL random hexamers at 150 ng/μL (Gene Link, Hawthorne, NY), 2 μL dNTP (each at 10 mM), and 1 μL SuperScript II (Invitrogen), followed by incubation at 42ºC for 2 h. We note that these RT parameters may be suboptimal to those described previously (*41, 42*). After RT, 25 μL water was added to each well to dilute cDNA, and the cDNA plates were stored at -20ºC for later use. The variable regions of heavy, kappa, and lambda chains were amplified independently by nested PCR in 50 μL, using 5 μL cDNA as template, with HotStarTaq Plus DNA polymerase (Qiagen) and primer mixes as described (*41, 43*). Cycler parameters were 94ºC for 5 m, 50 cycles of 94ºC for 30 s, 52-55ºC for 30 s, and 72ºC for 1 m, followed by 72ºC for 10 m. The PCR amplicons were subjected to direct Sanger sequencing, and the antibody sequences were analyzed using IMGT/V-QUEST. Selected PCR sequences that gave productive gamma,

kappa, and lambda chain rearrangements were re-amplified with custom primers containing unique restriction digest sites and cloned into the corresponding human gamma, kappa, and lambda chain expression vectors as described (*40-42*). Full IgG1 was expressed by co-transfecting Expi293F cells (ThermoFisher) with equal amounts of paired heavy and light chain plasmids and purified using recombinant Protein A agarose (ThermoFisher).

ELISA, with and without Endo H treatment

H7N9 HA and HA1 based on A/Shanghai/2/2013, A/Guangdong/17SF003/2016, A/Hong Kong/125/2017, and H7N7 HA based on A/Netherlands/219/2003 were purchased (Immune Technologies, New York, NY). Other non-H7 HA proteins were also purchased (Sino Biological, Chesterbrook, PA). ELISA plates were coated with HA or HA1 antigens at 2 μg/mL in PBS overnight at 4°C. For Endo H treatment, the required amount of antigen was diluted in 10x buffer and mixed with 1 μL Endo H (New England BioLabs, Ipswich, MA) for 1 h at 37ºC; an equal amount of antigen (untreated) was processed under identical condition without Endo H. Both treated and untreated antigens were then diluted in PBS to coat ELISA plates at 2 μg/mL. Coated plates were blocked with 1% BSA (bovine serum albumin) in PBS for 1 h at 37°C, followed by incubation with serially diluted mAbs for 1 h at 37°C. Horseradish peroxidase (HRP)-conjugated goat anti-human IgG Fc (Jackson ImmunoResearch, West Grove, PA) was added at 1:10,000 for 1 h at 37°C. All ELISA incubation volumes were 100 μL/well except that 200 μL/well was used for blocking. Plates were washed between steps with 0.1% Tween 20 in PBS and developed with 3,3′,5,5′-tetramethylbenzidine (TMB) (Novex, Life Technologies) for 5 m, with 1 M H_2SO_4 as terminator and read at 450 nm.

H7N9 neutralization assays

H7N9 neutralization was first measured with a single-round infection of MDCK cells using H7N9 2013 and 2016 pseudoviruses as described (*30*). Neutralization curves were fitted by a 5-parameter nonlinear regression built in Prism (GraphPad Software, La Jolla, CA). The 50% inhibitory titers (IC_{50}s) were reported as the antibody concentrations required to inhibit infection by 50%. H7N9 neutralization was next measured using live replicating influenza viruses to infect MDCK cells as described (*44*). Briefly, serially diluted mAbs were incubated with 100 $TCID_{50}$ (50% tissue culture infective dose) of an influenza virus at 37°C for 2 h, and 100 μL virus-mAb mixture was added to MDCK cells. After 1 h incubation, the virus-mAb mixture was removed, and minimum-essential medium with 2 μg/mL L-1-tosylamide-2-phenylethylchloromethyl ketone-treated trypsin (TPCK-trypsin) was added to each well. The plates were then incubated for 72 h, and cytopathic effects were recorded. The mAb concentration that protected 50% of 5 replicate wells from cytopathology was reported as IC_{50}.

H7 HA production

Soluble, disulfide-stabilized, fully cleaved H7 HA trimers were produced by transient co-transfection of plasmids encoding H7 HA (H7 SH13 DS2 6R) and Furin of Expi293F cells (Life Technologies) using Turbo293 transfection Reagent (Speed biosystem). After 5 days at 37˚C, culture supernatants were harvested by centrifugation and concentrated 5-fold by Tangential Flow Filtration. The recombinant HA trimer was captured by Ni-NTA (Sigma-Aldrich) through a C-terminal 6xHis-tag. The imidazole eluant was combined 1:1 (v/v) with saturated ammonium sulfate, centrifuged at 4˚C, and pellet removed. The supernatant was dialyzed against 500 mM NaCl, 50 mM Tris pH 8, and purified by size exclusion chromatography on a Superdex 200 Increase 10/300 GL column (Cytiva).

Human mAb Fab preparation

Human mAb Fab fragments were produced by digestion of the full IgG antibodies with immobilized Papain (ThermoFisher) equilibrated with 25 mM phosphate, 150 mM NaCl, pH 10, and 2 mM EDTA for 3 h. The resulting Fabs were purified from the cleaved Fc domain by affinity chromatography using protein A. Fab purity was analyzed by SDS-PAGE. All Fabs were buffer-exchanged into 25 mM phosphate, 150 mM NaCl, pH 7.0 prior to cryo-EM experiments.

Cryo-EM sample preparation, data collection, and structure determination

To determine the structures of H7.HK1 and H7.HK2 with H7 HA trimer, trimer was mixed with the antibody Fab at 1 to 1.2 molar ratio at a final total protein concentration of ~1 mg/mL and adjusted to a final concentration of 0.005% (w/v) n-Dodecyl β-D-maltoside (DDM) to prevent preferred orientation and aggregation during vitrification. Cryo-EM grids were prepared by applying 3 μL of sample to a freshly glow discharged carbon-coated copper grid (CF 1.2/1.3 300 mesh). The sample was vitrified in liquid ethane using a Vitrobot Mark IV with a wait time of 30 s, a blot time of 3 s, and a blot force of 0. Cryo-EM data were collected on a Titan Krios operating at 300 keV, equipped with a K3 detector (Gatan) operating in counting mode. Data were acquired using Leginon (*45*). The dose was fractionated over 50 raw frames. For all structures, the movie frames were aligned and dose-weighted (*46*) using cryoSPARC 3.4 (*47*); the CTF estimation, particle picking, 2D classifications, ab initio model generation, heterogeneous refinements, homogeneous 3D refinements and non-uniform refinement calculations were carried out using cryoSPARC 3.4 (*47*).

Atomic model building and refinement

For structural determination, a model of the antibody Fab was generated using SAbPred (*48*). The Fab model and the crystal structure of an H7 HA mutant (PDB: 6IDD) (*10*) was docked into the cryo-EM density map using UCSF Chimera (*49*) to build an initial model of the complex. The model was then manually rebuilt to the best fit into the density using Coot (*50*) and refined using Phenix (*51*). Interface calculations were performed using PISA (*52*). Structures were analyzed and figures were generated using PyMOL (http://www.pymol.org) and UCSF Chimera (*49*). Final model statistics are summarized in **Table S1**.

Mouse prophylactic and therapeutic studies

The mouse prophylactic and therapeutic studies were approved by the Committee on the Use of Live Animals in Teaching and Research (CULATR) of the University of Hong Kong (Reference number: 4011-16) and conducted in biosafety level 3 animal facilities as described previously (*53*). Female BALB/c mice of 6-8 weeks of age were obtained from the Laboratory Animal Unit of The University of Hong Kong. For prophylactic study, one day before virus inoculation, each mouse was administered with 100 μL of mAb at 1 mg/mL intraperitoneally. For therapeutic study, infected mice were administered with 100 μL of mAb at 1 mg/mL intraperitoneally at day 1 post viral challenge. Mice in the control groups were administered with either PBS or with a non-H7N9 mAb. On the day of virus infection, each mouse was inoculated with 10 LD_{50} (40 μL) of H7N9/AH1 virus through intranasal route. Virus inoculation was performed under ketamine (100 mg/kg) and xylazine (10 mg/kg) anesthesia. The mice were monitored for 14 days with disease severity score and body weight recorded daily. Disease severity were scored as follow: Score 0, apparently healthy; Score 1 (mild disease symptom), ruffled fur but still active; Score 2

(medium disease symptom), ruffled fur, reduced activity and no weight gain; Score 3 (severe disease symptoms), ruffled fur, hunched posture, labored breathing and weight loss; Score 4 (moribund): very inactive, showing difficulty moving around and accessing to food and water, and weight loss. The predefined humane endpoints were either a weight loss of ≥ 20% or a disease severity score of 4. Mice were euthanized if the humane endpoints were reached.

Statistical analysis

GraphPad Prism was used to plot the ELISA data using sigmoidal dose-response with variable slope for curve fitting and the neutralization data using 5-parameter nonlinear regression for curve fitting. All quantitative data are presented as mean ± standard error (SEM). GraphPad Prism was also used to plot the mouse Survival curves. Unpaired student's t-test in GraphPad Prism was used for comparisons between groups, and a *P* value of less than 0.05 was considered statistically significant.

Data availability

Sequences of the heavy and light chain variable regions of four H7N9 human mAbs are available in GenBank under accession # xxxxxxxx to xxxxxxxx. The Cryo-EM reconstruction of H7.HK1 and H7.HK2 Fabs in complex with H7 SH13 DS2 6R HA has been deposited in the Electron Microscopy Data Bank as EMD-41422 and EMD-41441 and the Protein Data Bank (PDB: 8TNL and 8TOA). Materials will be made available to researchers with appropriate materials transfer agreements (MTAs). All inquiries should be sent to the corresponding authors.

References

1. R. Gao, B. Cao, Y. Hu, Z. Feng, D. Wang, W. Hu, J. Chen, Z. Jie, H. Qiu, K. Xu, X. Xu, H. Lu, W. Zhu, Z. Gao, N. Xiang, Y. Shen, Z. He, Y. Gu, Z. Zhang, Y. Yang, X. Zhao, L. Zhou, X. Li, S. Zou, Y. Zhang, X. Li, L. Yang, J. Guo, J. Dong, Q. Li, L. Dong, Y. Zhu, T. Bai, S. Wang, P. Hao, W. Yang, Y. Zhang, J. Han, H. Yu, D. Li, G. F. Gao, G. Wu, Y. Wang, Z. Yuan, Y. Shu, Human infection with a novel avian-origin influenza A (H7N9) virus. *N Engl J Med* **368**, 1888-1897 (2013).
2. C. J. Bao, L. B. Cui, M. H. Zhou, L. Hong, G. F. Gao, H. Wang, Live-animal markets and influenza A (H7N9) virus infection. *N Engl J Med* **368**, 2337-2339 (2013).
3. Y. Chen, W. Liang, S. Yang, N. Wu, H. Gao, J. Sheng, H. Yao, J. Wo, Q. Fang, D. Cui, Y. Li, X. Yao, Y. Zhang, H. Wu, S. Zheng, H. Diao, S. Xia, K. H. Chan, H. W. Tsoi, J. L. Teng, W. Song, P. Wang, S. Y. Lau, M. Zheng, J. F. Chan, K. K. To, H. Chen, L. Li, K. Y. Yuen, Human infections with the emerging avian influenza A H7N9 virus from wet market poultry: clinical analysis and characterisation of viral genome. *Lancet* **381**, 1916-1925 (2013).
4. S. Su, M. Gu, D. Liu, J. Cui, G. F. Gao, J. Zhou, X. Liu, Epidemiology, Evolution, and Pathogenesis of H7N9 Influenza Viruses in Five Epidemic Waves since 2013 in China. *Trends Microbiol* **25**, 713-728 (2017).
5. X. Wang, H. Jiang, P. Wu, T. M. Uyeki, L. Feng, S. Lai, L. Wang, X. Huo, K. Xu, E. Chen, X. Wang, J. He, M. Kang, R. Zhang, J. Zhang, J. Wu, S. Hu, H. Zhang, X. Liu, W. Fu, J. Ou, S. Wu, Y. Qin, Z. Zhang, Y. Shi, J. Zhang, J. Artois, V. J. Fang, H. Zhu, Y. Guan, M. Gilbert, P. W. Horby, G. M. Leung, G. F. Gao, B. J. Cowling, H. Yu, Epidemiology of avian influenza A H7N9 virus in human beings across five epidemics in mainland China, 2013-17: an epidemiological study of laboratory-confirmed case series. *The Lancet. Infectious diseases* **17**, 822-832 (2017).
6. W. Qi, W. Jia, D. Liu, J. Li, Y. Bi, S. Xie, B. Li, T. Hu, Y. Du, L. Xing, J. Zhang, F. Zhang, X. Wei, J. S. Eden, H. Li, H. Tian, W. Li, G. Su, G. Lao, C. Xu, B. Xu, W. Liu, G. Zhang, T. Ren, E. C. Holmes, J. Cui, W. Shi, G. F. Gao, M. Liao, Emergence and Adaptation of a Novel Highly Pathogenic H7N9 Influenza Virus in Birds and Humans from a 2013 Human-Infecting Low-Pathogenic Ancestor. *Journal of virology* **92**, (2018).
7. J. Zhou, D. Wang, R. Gao, B. Zhao, J. Song, X. Qi, Y. Zhang, Y. Shi, L. Yang, W. Zhu, T. Bai, K. Qin, Y. Lan, S. Zou, J. Guo, J. Dong, L. Dong, Y. Zhang, H. Wei, X. Li, J. Lu, L. Liu, X. Zhao, X. Li, W. Huang, L. Wen, H. Bo, L. Xin, Y. Chen, C. Xu, Y. Pei, Y. Yang, X. Zhang, S. Wang, Z. Feng, J. Han, W. Yang, G. F. Gao, G. Wu, D. Li, Y. Wang, Y. Shu, Biological features of novel avian influenza A (H7N9) virus. *Nature* **499**, 500-503 (2013).
8. Y. Shi, W. Zhang, F. Wang, J. Qi, Y. Wu, H. Song, F. Gao, Y. Bi, Y. Zhang, Z. Fan, C. Qin, H. Sun, J. Liu, J. Haywood, W. Liu, W. Gong, D. Wang, Y. Shu, Y. Wang, J. Yan, G. F. Gao, Structures and receptor binding of hemagglutinins from human-infecting H7N9 influenza viruses. *Science* **342**, 243-247 (2013).
9. R. Xu, R. P. de Vries, X. Zhu, C. M. Nycholat, R. McBride, W. Yu, J. C. Paulson, I. A. Wilson, Preferential recognition of avian-like receptors in human influenza A H7N9 viruses. *Science* **342**, 1230-1235 (2013).

10. Y. Xu, R. Peng, W. Zhang, J. Qi, H. Song, S. Liu, H. Wang, M. Wang, H. Xiao, L. Fu, Z. Fan, Y. Bi, J. Yan, Y. Shi, G. F. Gao, Avian-to-Human Receptor-Binding Adaptation of Avian H7N9 Influenza Virus Hemagglutinin. *Cell Rep* **29**, 2217-2228 e2215 (2019).
11. Y. Hu, S. Lu, Z. Song, W. Wang, P. Hao, J. Li, X. Zhang, H. L. Yen, B. Shi, T. Li, W. Guan, L. Xu, Y. Liu, S. Wang, X. Zhang, D. Tian, Z. Zhu, J. He, K. Huang, H. Chen, L. Zheng, X. Li, J. Ping, B. Kang, X. Xi, L. Zha, Y. Li, Z. Zhang, M. Peiris, Z. Yuan, Association between adverse clinical outcome in human disease caused by novel influenza A H7N9 virus and sustained viral shedding and emergence of antiviral resistance. *Lancet* **381**, 2273-2279 (2013).
12. R. Hai, M. Schmolke, V. H. Leyva-Grado, R. R. Thangavel, I. Margine, E. L. Jaffe, F. Krammer, A. Solorzano, A. Garcia-Sastre, P. Palese, N. M. Bouvier, Influenza A(H7N9) virus gains neuraminidase inhibitor resistance without loss of in vivo virulence or transmissibility. *Nature communications* **4**, 2854 (2013).
13. H. Marjuki, V. P. Mishin, A. P. Chesnokov, J. A. De La Cruz, C. T. Davis, J. M. Villanueva, A. M. Fry, L. V. Gubareva, Neuraminidase Mutations Conferring Resistance to Oseltamivir in Influenza A(H7N9) Viruses. *Journal of virology* **89**, 5419-5426 (2015).
14. K. K. To, W. Song, S. Y. Lau, T. L. Que, D. C. Lung, I. F. Hung, H. Chen, K. Y. Yuen, Unique reassortant of influenza A(H7N9) virus associated with severe disease emerging in Hong Kong. *The Journal of infection* **69**, 60-68 (2014).
15. P. L. Ho, W. C. Sin, J. F. Chan, V. C. Cheng, K. H. Chan, Severe influenza A H7N9 pneumonia with rapid virological response to intravenous zanamivir. *The European respiratory journal* **44**, 535-537 (2014).
16. M. Kiso, S. Yamayoshi, Y. Furusawa, M. Imai, Y. Kawaoka, Treatment of Highly Pathogenic H7N9 Virus-Infected Mice with Baloxavir Marboxil. *Viruses* **11**, (2019).
17. K. A. Huang, P. Rijal, H. Jiang, B. Wang, L. Schimanski, T. Dong, Y. M. Liu, P. Chang, M. Iqbal, M. C. Wang, Z. Chen, R. Song, C. C. Huang, J. H. Yang, J. Qi, T. Y. Lin, A. Li, T. J. Powell, J. T. Jan, C. Ma, G. F. Gao, Y. Shi, A. R. Townsend, Structure-function analysis of neutralizing antibodies to H7N9 influenza from naturally infected humans. *Nat Microbiol* **4**, 306-315 (2019).
18. Z. Chen, J. Wang, L. Bao, L. Guo, W. Zhang, Y. Xue, H. Zhou, Y. Xiao, F. Wu, Y. Deng, C. Qin, Q. Jin, Human monoclonal antibodies targeting the haemagglutinin glycoprotein can neutralize H7N9 influenza virus. *Nature communications* **6**, 6714 (2015).
19. N. J. Thornburg, H. Zhang, S. Bangaru, G. Sapparapu, N. Kose, R. M. Lampley, R. G. Bombardi, Y. Yu, S. Graham, A. Branchizio, S. M. Yoder, M. T. Rock, C. B. Creech, K. M. Edwards, D. Lee, S. Li, I. A. Wilson, A. Garcia-Sastre, R. A. Albrecht, J. E. Crowe, Jr., H7N9 influenza virus neutralizing antibodies that possess few somatic mutations. *The Journal of clinical investigation* **126**, 1482-1494 (2016).
20. C. J. Henry Dunand, P. E. Leon, M. Huang, A. Choi, V. Chromikova, I. Y. Ho, G. S. Tan, J. Cruz, A. Hirsh, N. Y. Zheng, C. E. Mullarkey, F. A. Ennis, M. Terajima, J. J. Treanor, D. J. Topham, K. Subbarao, P. Palese, F. Krammer, P. C. Wilson, Both Neutralizing and Non-Neutralizing Human H7N9 Influenza Vaccine-Induced Monoclonal Antibodies Confer Protection. *Cell host & microbe* **19**, 800-813 (2016).
21. S. Bangaru, S. Lang, M. Schotsaert, H. A. Vanderven, X. Zhu, N. Kose, R. Bombardi, J. A. Finn, S. J. Kent, P. Gilchuk, I. Gilchuk, H. L. Turner, A. Garcia-Sastre, S. Li, A. B.

Ward, I. A. Wilson, J. E. Crowe, Jr., A Site of Vulnerability on the Influenza Virus Hemagglutinin Head Domain Trimer Interface. *Cell* **177**, 1136-1152 e1118 (2019).
22. J. Wang, Z. Chen, L. Bao, W. Zhang, Y. Xue, X. Pang, X. Zhang, C. Qin, Q. Jin, Characterization of Two Human Monoclonal Antibodies Neutralizing Influenza A H7N9 Viruses. *Journal of virology* **89**, 9115-9118 (2015).
23. R. G. Webster, W. G. Laver, Determination of the number of nonoverlapping antigenic areas on Hong Kong (H3N2) influenza virus hemagglutinin with monoclonal antibodies and the selection of variants with potential epidemiological significance. *Virology* **104**, 139-148 (1980).
24. J. J. Skehel, D. J. Stevens, R. S. Daniels, A. R. Douglas, M. Knossow, I. A. Wilson, D. C. Wiley, A carbohydrate side chain on hemagglutinins of Hong Kong influenza viruses inhibits recognition by a monoclonal antibody. *Proc Natl Acad Sci U S A* **81**, 1779-1783 (1984).
25. L. Popova, K. Smith, A. H. West, P. C. Wilson, J. A. James, L. F. Thompson, G. M. Air, Immunodominance of antigenic site B over site A of hemagglutinin of recent H3N2 influenza viruses. *PloS one* **7**, e41895 (2012).
26. W. Zhu, J. Zhou, Z. Li, L. Yang, X. Li, W. Huang, S. Zou, W. Chen, H. Wei, J. Tang, L. Liu, J. Dong, D. Wang, Y. Shu, Biological characterisation of the emerged highly pathogenic avian influenza (HPAI) A(H7N9) viruses in humans, in mainland China, 2016 to 2017. *Euro Surveill* **22**, (2017).
27. J. C. Kile, R. Ren, L. Liu, C. M. Greene, K. Roguski, A. D. Iuliano, Y. Jang, J. Jones, S. Thor, Y. Song, S. Zhou, S. C. Trock, V. Dugan, D. E. Wentworth, M. Z. Levine, T. M. Uyeki, J. M. Katz, D. B. Jernigan, S. J. Olsen, A. M. Fry, E. Azziz-Baumgartner, C. T. Davis, Update: Increase in Human Infections with Novel Asian Lineage Avian Influenza A(H7N9) Viruses During the Fifth Epidemic - China, October 1, 2016-August 7, 2017. *MMWR Morb Mortal Wkly Rep* **66**, 928-932 (2017).
28. F. Nimmerjahn, J. V. Ravetch, Divergent immunoglobulin g subclass activity through selective Fc receptor binding. *Science* **310**, 1510-1512 (2005).
29. S. J. Gamblin, J. J. Skehel, Influenza hemagglutinin and neuraminidase membrane glycoproteins. *J Biol Chem* **285**, 28403-28409 (2010).
30. C. Qiu, Y. Huang, A. Zhang, D. Tian, Y. Wan, X. Zhang, W. Zhang, Z. Zhang, Z. Yuan, Y. Hu, J. Xu, Safe pseudovirus-based assay for neutralization antibodies against influenza A(H7N9) virus. *Emerging infectious diseases* **19**, 1685-1687 (2013).
31. D. Corti, J. Voss, S. J. Gamblin, G. Codoni, A. Macagno, D. Jarrossay, S. G. Vachieri, D. Pinna, A. Minola, F. Vanzetta, C. Silacci, B. M. Fernandez-Rodriguez, G. Agatic, S. Bianchi, I. Giacchetto-Sasselli, L. Calder, F. Sallusto, P. Collins, L. F. Haire, N. Temperton, J. P. Langedijk, J. J. Skehel, A. Lanzavecchia, A neutralizing antibody selected from plasma cells that binds to group 1 and group 2 influenza A hemagglutinins. *Science* **333**, 850-856 (2011).
32. C. Chothia, A. M. Lesk, Canonical structures for the hypervariable regions of immunoglobulins. *J Mol Biol* **196**, 901-917 (1987).
33. C. Chothia, A. M. Lesk, A. Tramontano, M. Levitt, S. J. Smith-Gill, G. Air, S. Sheriff, E. A. Padlan, D. Davies, W. R. Tulip, et al., Conformations of immunoglobulin hypervariable regions. *Nature* **342**, 877-883 (1989).
34. B. Al-Lazikani, A. M. Lesk, C. Chothia, Standard conformations for the canonical structures of immunoglobulins. *J Mol Biol* **273**, 927-948 (1997).

35. X. Xiong, S. R. Martin, L. F. Haire, S. A. Wharton, R. S. Daniels, M. S. Bennett, J. W. McCauley, P. J. Collins, P. A. Walker, J. J. Skehel, S. J. Gamblin, Receptor binding by an H7N9 influenza virus from humans. *Nature* **499**, 496-499 (2013).
36. C. S. Cheung, J. Gorman, S. F. Andrews, R. Rawi, M. Reveiz, C. H. Shen, Y. Wang, D. R. Harris, A. F. Nazzari, A. S. Olia, J. Raab, I. T. Teng, R. Verardi, S. Wang, Y. Yang, G. Y. Chuang, A. B. McDermott, T. Zhou, P. D. Kwong, Structure of an influenza group 2-neutralizing antibody targeting the hemagglutinin stem supersite. *Structure* **30**, 993-1003 e1006 (2022).
37. C. Jiao, B. Wang, P. Chen, Y. Jiang, J. Liu, Analysis of the conserved protective epitopes of hemagglutinin on influenza A viruses. *Front Immunol* **14**, 1086297 (2023).
38. D. J. DiLillo, G. S. Tan, P. Palese, J. V. Ravetch, Broadly neutralizing hemagglutinin stalk-specific antibodies require FcgammaR interactions for protection against influenza virus in vivo. *Nature medicine* **20**, 143-151 (2014).
39. E. Benjamin, W. Wang, J. M. McAuliffe, F. J. Palmer-Hill, N. L. Kallewaard, Z. Chen, J. A. Suzich, W. S. Blair, H. Jin, Q. Zhu, A broadly neutralizing human monoclonal antibody directed against a novel conserved epitope on the influenza virus H3 hemagglutinin globular head. *Journal of virology* **88**, 6743-6750 (2014).
40. M. Jia, H. Lu, M. Markowitz, C. Cheng-Mayer, X. Wu, Development of Broadly Neutralizing Antibodies and Their Mapping by Monomeric gp120 in Human Immunodeficiency Virus Type 1-Infected Humans and Simian-Human Immunodeficiency Virus SHIVSF162P3N-Infected Macaques. *Journal of virology* **90**, 4017-4031 (2016).
41. T. Tiller, E. Meffre, S. Yurasov, M. Tsuiji, M. C. Nussenzweig, H. Wardemann, Efficient generation of monoclonal antibodies from single human B cells by single cell RT-PCR and expression vector cloning. *J Immunol Methods* **329**, 112-124 (2008).
42. X. Wu, Z. Y. Yang, Y. Li, C. M. Hogerkorp, W. R. Schief, M. S. Seaman, T. Zhou, S. D. Schmidt, L. Wu, L. Xu, N. S. Longo, K. McKee, S. O'Dell, M. K. Louder, D. L. Wycuff, Y. Feng, M. Nason, N. Doria-Rose, M. Connors, P. D. Kwong, M. Roederer, R. T. Wyatt, G. J. Nabel, J. R. Mascola, Rational design of envelope identifies broadly neutralizing human monoclonal antibodies to HIV-1. *Science* **329**, 856-861 (2010).
43. J. F. Scheid, H. Mouquet, B. Ueberheide, R. Diskin, F. Klein, T. Y. Oliveira, J. Pietzsch, D. Fenyo, A. Abadir, K. Velinzon, A. Hurley, S. Myung, F. Boulad, P. Poignard, D. R. Burton, F. Pereyra, D. D. Ho, B. D. Walker, M. S. Seaman, P. J. Bjorkman, B. T. Chait, M. C. Nussenzweig, Sequence and structural convergence of broad and potent HIV antibodies that mimic CD4 binding. *Science* **333**, 1633-1637 (2011).
44. K. K. To, A. J. Zhang, I. F. Hung, T. Xu, W. C. Ip, R. T. Wong, J. C. Ng, J. F. Chan, K. H. Chan, K. Y. Yuen, High titer and avidity of nonneutralizing antibodies against influenza vaccine antigen are associated with severe influenza. *Clinical and vaccine immunology : CVI* **19**, 1012-1018 (2012).
45. A. Cheng, C. Negro, J. F. Bruhn, W. J. Rice, S. Dallakyan, E. T. Eng, D. G. Waterman, C. S. Potter, B. Carragher, Leginon: New features and applications. *Protein Sci* **30**, 136-150 (2021).
46. S. Q. Zheng, E. Palovcak, J. P. Armache, K. A. Verba, Y. Cheng, D. A. Agard, MotionCor2: anisotropic correction of beam-induced motion for improved cryo-electron microscopy. *Nat Methods* **14**, 331-332 (2017).

47. A. Punjani, J. L. Rubinstein, D. J. Fleet, M. A. Brubaker, cryoSPARC: algorithms for rapid unsupervised cryo-EM structure determination. *Nat Methods* **14**, 290-296 (2017).
48. J. Dunbar, K. Krawczyk, J. Leem, C. Marks, J. Nowak, C. Regep, G. Georges, S. Kelm, B. Popovic, C. M. Deane, SAbPred: a structure-based antibody prediction server. *Nucleic Acids Res* **44**, W474-478 (2016).
49. E. F. Pettersen, T. D. Goddard, C. C. Huang, G. S. Couch, D. M. Greenblatt, E. C. Meng, T. E. Ferrin, UCSF Chimera--a visualization system for exploratory research and analysis. *J Comput Chem* **25**, 1605-1612 (2004).
50. A. Casanal, B. Lohkamp, P. Emsley, Current developments in Coot for macromolecular model building of Electron Cryo-microscopy and Crystallographic Data. *Protein Sci* **29**, 1069-1078 (2020).
51. P. D. Adams, K. Gopal, R. W. Grosse-Kunstleve, L. W. Hung, T. R. Ioerger, A. J. McCoy, N. W. Moriarty, R. K. Pai, R. J. Read, T. D. Romo, J. C. Sacchettini, N. K. Sauter, L. C. Storoni, T. C. Terwilliger, Recent developments in the PHENIX software for automated crystallographic structure determination. *J Synchrotron Radiat* **11**, 53-55 (2004).
52. E. Krissinel, K. Henrick, Inference of macromolecular assemblies from crystalline state. *J Mol Biol* **372**, 774-797 (2007).
53. K. K. To, A. J. Zhang, A. S. Chan, C. Li, J. P. Cai, C. C. Lau, C. G. Li, A. S. Jahan, W. L. Wu, L. Li, A. K. Tsang, K. H. Chan, H. Chen, K. Y. Yuen, Recombinant influenza A virus hemagglutinin HA2 subunit protects mice against influenza A(H7N9) virus infection. *Archives of virology* **160**, 777-786 (2015).

Acknowledgments

We thank the patient for donating blood for the study. We thank Reda Rawi and Jeffrey C. Boyington for design of H7 SH13 DS2 6R used for structural analysis. Cryo-EM data were collected at the Columbia University Cryo-Electron Microscopy Center. We thank Shuofeng Yuan and Vincent Poon for assistance with the animal experiments.

Funding

- U.S. Department of Defense contract No. W911NF-14-C-0001 (DDH and XW)
- Health@InnoHK, Innovation and Technology Commission of Hong Kong (KY and KKT)
- Donations from Richard Yu and Carol Yu, Shaw Foundation Hong Kong, Michael Seak-Kan Tong, The Hui Ming, Hui Hoy and Chow Sin Lan Charity Fund Limited, Chan Yin Chuen Memorial Charitable Foundation, Marina Man-Wai Lee, Jessie and George Ho Charitable Foundation, Kai Chong Tong, Tse Kam Ming Laurence, Foo Oi Foundation Limited, Betty Hing-Chu Lee, and Ping Cham So (KY and KKT)
- Bill and Melinda Gates Foundation grants FNIH SHAP19IUFV (LS) and INV-016167 (LS)
- National Institutes of Health, National Institute of Allergy and Infectious Disease, Intramural Research Program of the Vaccine Research Center (PDK)

Author contributions

Conceptualization: XW, DDH, KY
Methodology: XW, KKT, LS
Investigation: MJ, HZ, NCM, HL, YL, HD, JEB
Visualization: XW, NCM
Funding acquisition: DDH, XW, KY, KKT, LS, PDK
Project administration: XW, KKT
Supervision: XW, KKT, KY, PDK, LS
Writing – original draft: XW, KKT, NCM
Writing – review & editing: XW, KKT, MJ, HZ, NCM, KY, DDH, PDK, LS

Competing interests

An U.S. provisional patent titled “Human Protective Neutralizing and Non-neutralizing Antibodies and Their Use against Influenza Viruses” was filed with filing No. 63/578,505 and XW, MJ, NCM, HL, DDH, KY, KKT, PDK, and LS as co-inventors.

Additional information

Supplementary Figs. 1 to 4
Table S1

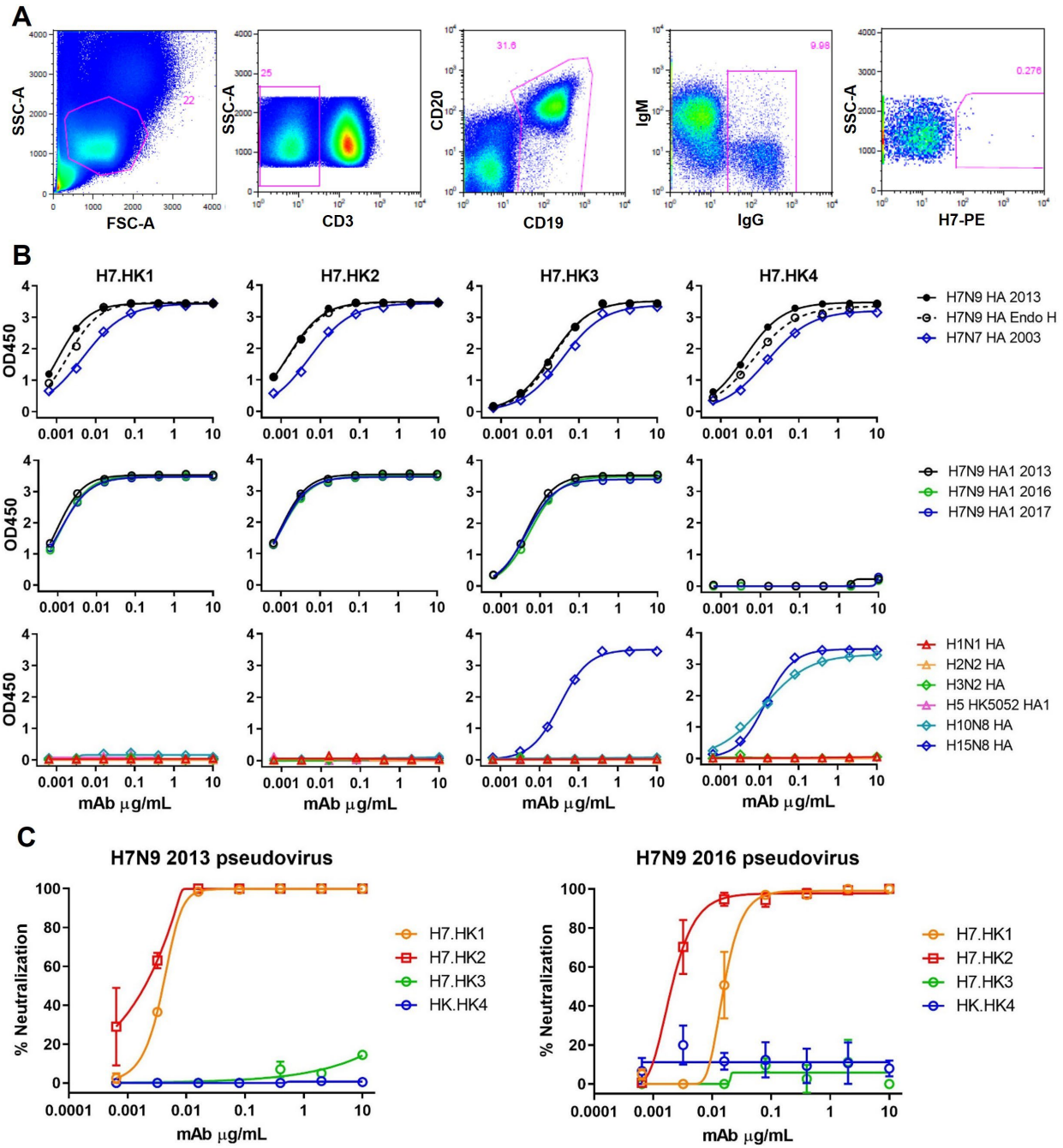

Fig. 1 Isolation and characterization of human H7N9 mAbs *in vitro*. (**A**) FACS depicting the staining and selection of H7-specific B cells from donor H7N9.HK2013 PBMCs 1 year post recovery. SSC-A, side scatter area; FSC-A, forward scatter area. (**B**) ELISA binding curves of the indicated mAbs to soluble recombinant H7N9 HA and H7N7 HA (upper panels), with or without Endo H treatment, to the matching H7N9 HA1 from 2013 or HA1s from 2016 and 2017 (middle panels), and to 6 other non-H7 HA or HA1 proteins (lower panels). (**C**) Neutralization curves of H7.HK mAbs against H7N9 2013 (left) and 2016 (right) pseudoviruses infecting MDCK cells. Data shown are mean ± SEM.

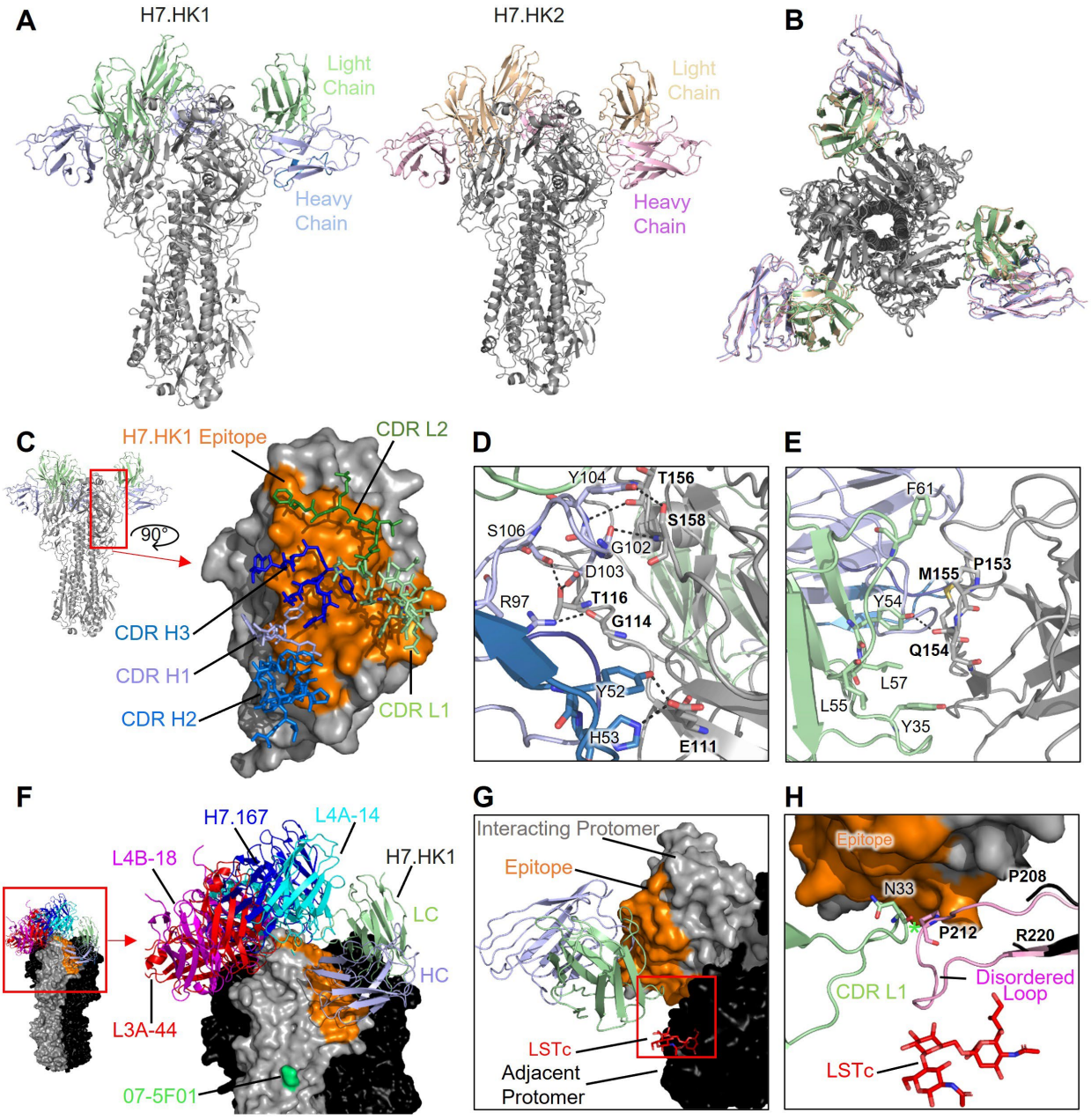

Fig. 2 Structural analysis of H7.HK1 and H7.HK2 in complex with H7 HA trimer. (**A**) Cryo-EM structures of H7.HK1 and H7.HK2 bound to H7 HA in the head region. (**B**) Top view of alignment of H7.HK1 and H7.HK2 complex structures. (**C**) Surface presentation of the H7.HK1 epitope (orange) on H7 HA1, with interacting CDRs shown. (**D**) H7.HK1 heavy chain forms seven hydrogen bonds and one salt bridge with H7 HA1. (**E**) H7.HK1 light chain forms one additional hydrogen bond with H7 HA1, and the interactions are stabilized by hydrophobic residues on the periphery of the light chain interface. (**F**) Modeling published structures of H7 HA1-binding antibodies (PDB: 6II4, 6II8, 6II9, 5V2A) onto the H7.HK1 bound structure, with an escape mutation R47K (green) reported for mAb 07-5F01. (**G**) Modeling the binding site of human receptor analogue LSTc (red) based on a previous crystal structure (PDB: 4BSE) onto H7 from the H7.HK1 complex, showing that H7.HK1 does not compete with sialic acid on the adjacent protomer (black). (**H**) Alignment of the H7.HK1 complex with a previous crystal structure of H7 (PDB: 4BSE) shows that the 220-loop (pink) required for sialic acid binding (G209-G219) is disorder in the complex structure and would clash with the H7.HK1 light chain if it were present. Green asterisk symbol denotes the <2 Å clash between the CDR L1 N33 and the predicted location of P212 on HA1.

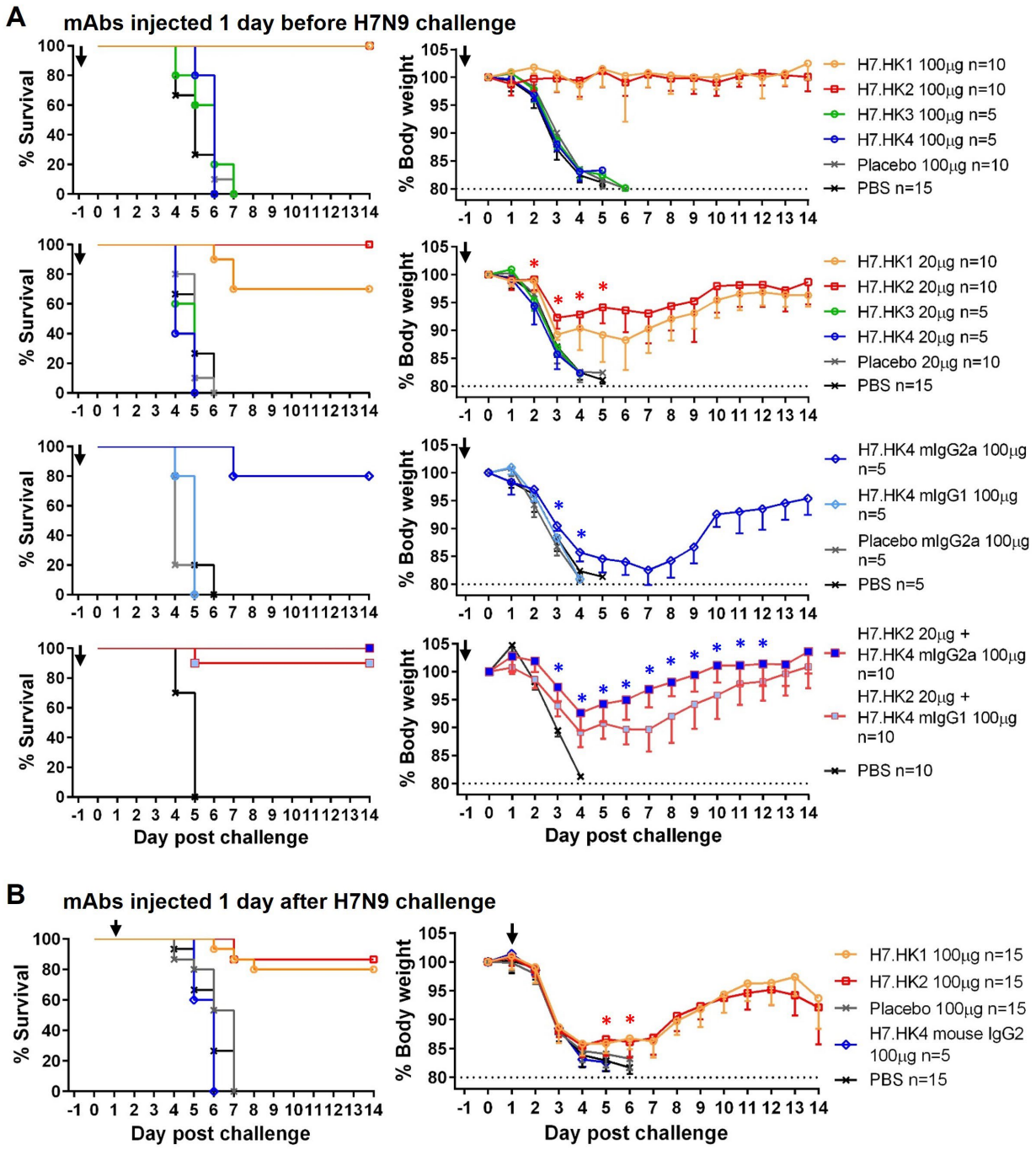

Fig. 3 Prophylactic and therapeutic effects of human H7N9 mAbs in mice i.n. challenged with 10 LD_{50} of A/Anhui/1/2013 H7N9. (**A**) Mice were i.p. injected with 100 μg (equivalent of 5 mg/kg) or 20 μg (equivalent of 1 mg/kg) of the indicated mAbs (as human IgG1 unless otherwise specified) one day before viral challenge; % survival (less than 20% weight loss) and % body weight of survived mice were plotted over time. (**B**) Mice were i.p. injected with 100 μg of the indicated mAbs one day after viral challenge; % survival and % body weight of survived mice were plotted over time. Arrows indicate the time when mAbs were administered. Control groups of a non-H7 placebo mAb and PBS were included. Data for each group were combined from 1-2 experiments and shown as mean – SEM. Asterisk symbols denote statistical significance with *P* values < 0.05.

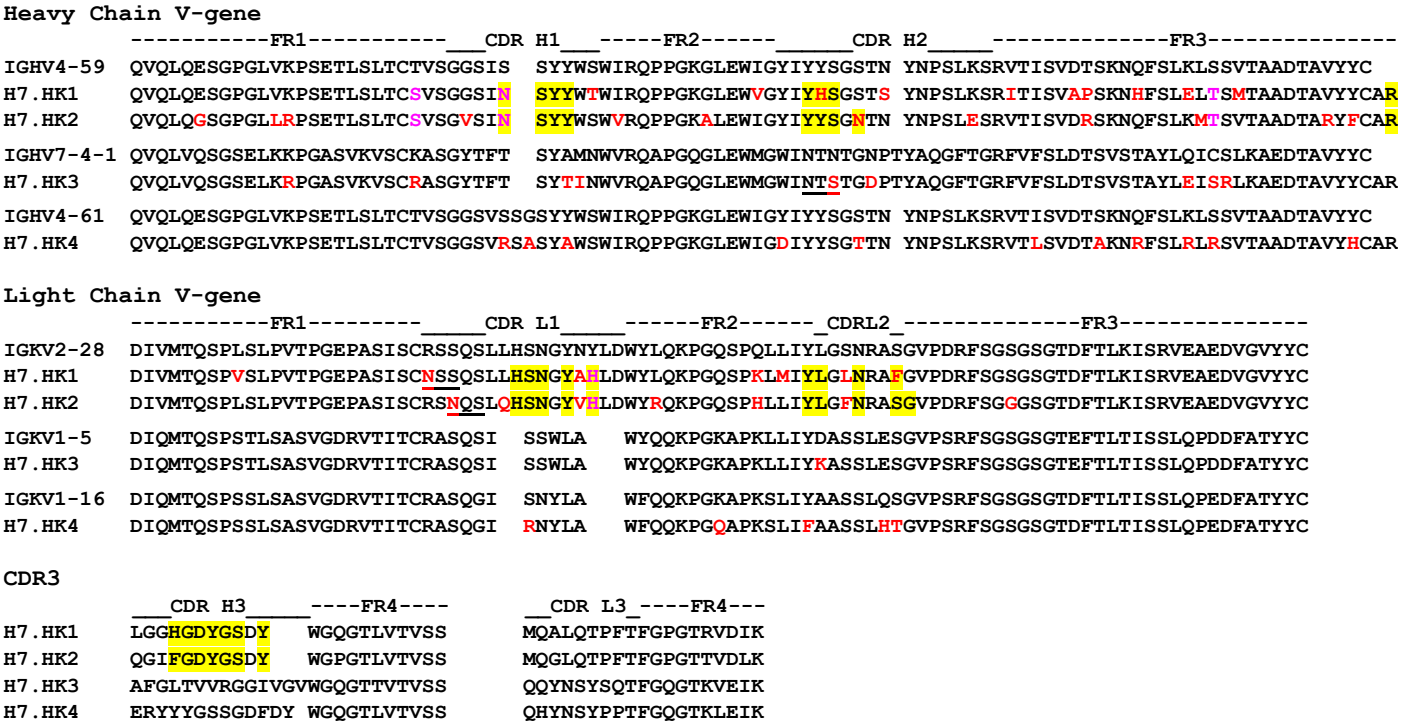

Supplementary Fig. 1 H7.HK mAb sequences. Protein sequences of the heavy and light chain variable regions of the H7.HK mAbs are aligned to the putative germline V-genes at top, with amino acid substitutions in red, and in magenta for substitutions shared between the clonally related mAbs H7.HK1 and H7.HK2. Spaces are added to maintain alignment; framework regions (FR) and complementarity-determining regions (CDRs) are indicated based on the Chothia nomenclature. Highlighted in yellow are the mAb residues (paratopes of H7.HK1 and H7.HK2) contacting the H7 antigen. The putative N-linked glycosylation sites on the light chain CDR L1 of H7.HK1 and H7.HK2 and the heavy chain CDR H2 of H7.HK3 are underlined.

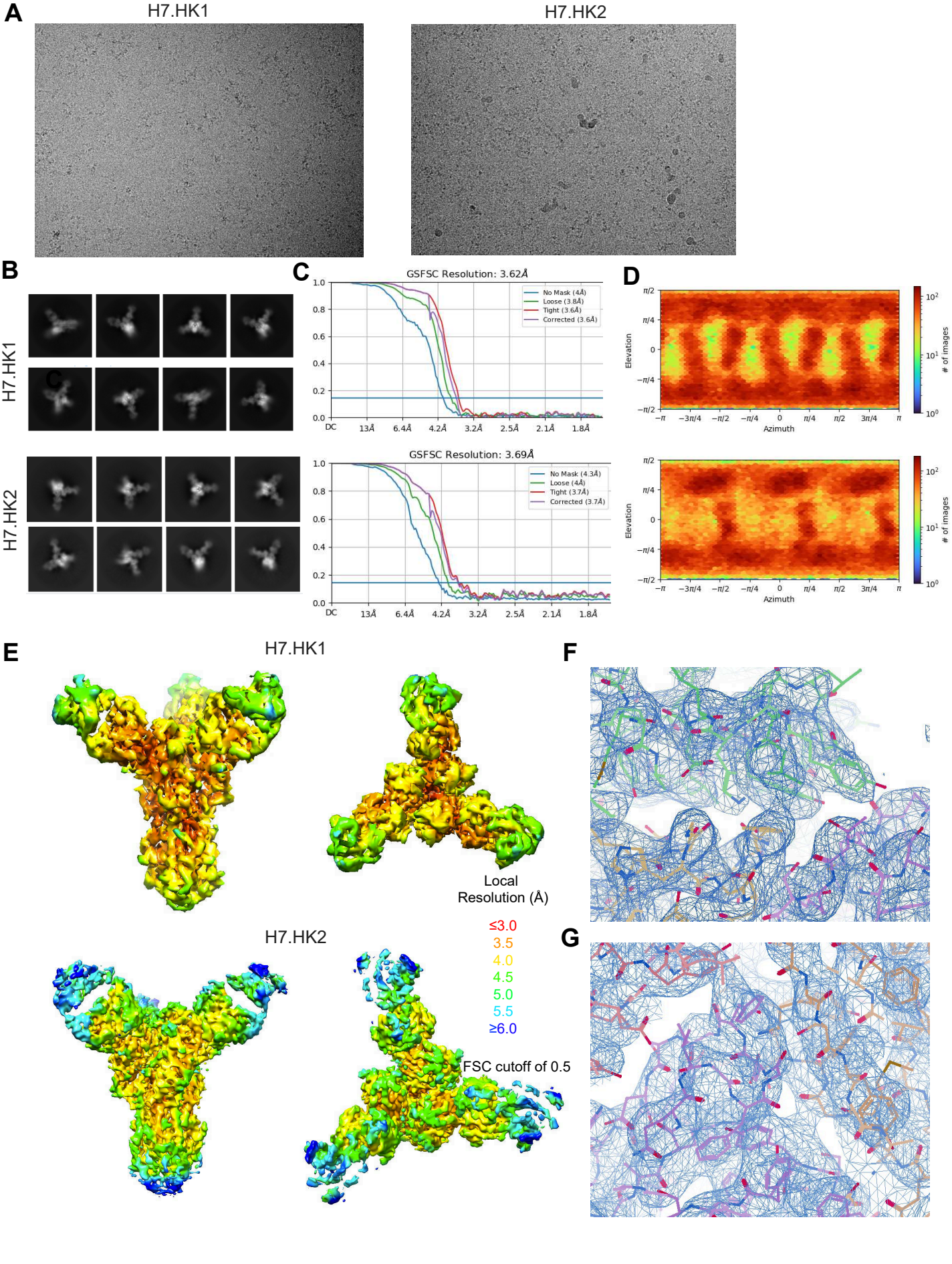
A
H7.HK1
H7.HK2
B
H7.HK1
H7.HK2
C
GSFSC Resolution: 3.62Å
No Mask (4Å)
Loose (3.8Å)
Tight (3.6Å)
Corrected (3.6Å)
DC
13Å
6.4Å
4.2Å
3.2Å
2.5Å
2.1Å
1.8Å
GSFSC Resolution: 3.69Å
No Mask (4.3Å)
Loose (4Å)
Tight (3.7Å)
Corrected (3.7Å)
D
Elevation
Azimuth
# of images
E
H7.HK1
H7.HK2
Local Resolution (Å)
≤3.0
3.5
4.0
4.5
5.0
5.5
≥6.0
FSC cutoff of 0.5
F
G

Supplementary Fig. 2 Cryo-EM details of H7.HK1 and H7.HK2 in complex with H7 SH13 DS2 6R HA trimer. (**A**) Representative micrograph of H7.HK1 (left) and H7.HK2 (right). (**B**) Representative 2D class averages of H7.HK1 and H7.HK2. (**C**) The gold-standard Fourier Shell Correlation (FSC) resulted in a resolution of 3.62 Å for the overall map of H7.HK1 and 3.69 Å for the overall map of H7.HK2. Non-uniform refinement with C3 symmetry was used for both reconstructions. (**D**) The orientations of all particles used in the final refinement are shown as a heatmap. (**E**) The local resolution of the final overall map is shown contoured at 0.0989 for both structures. Resolution estimation was generated through cryoSPARC using an FSC cutoff of 0.5. (**F**) Representative density is shown for the interface of H7.HK1 heavy chain, light chain, and H7 HA. (**G**) Representative density is shown for the interface of H7.HK2 heavy chain, light chain, and H7 HA.

A

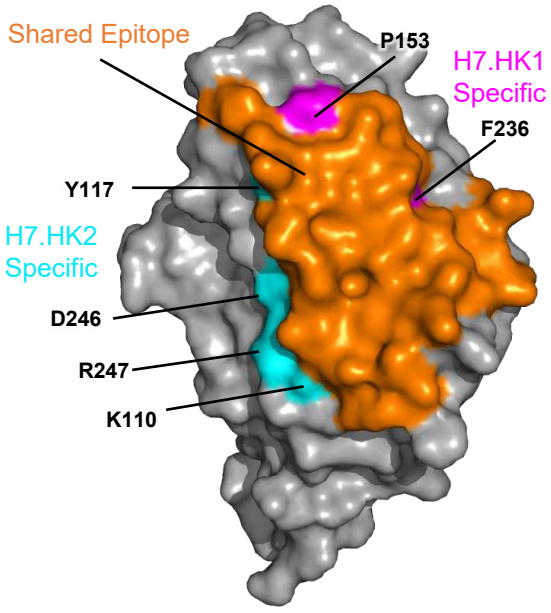

B

	H7.HK1 : H7	H7.HK2 : H7
Heavy Chain H Bonds	Y52 : **E111**	Y52 : **Y159**
	R97 : **G114**	R97 : **G114**
	G102 : **S158**	G102 : **S158**
	D103 : **T116**	D103 : **T116**
	Y104 : **T156**	Y104 : **T156**
	Y104 : **S158**	Y104 : **S158**
	S106 : **T116**	S106 : **T116**
Heavy Chain Salt Bridge	H53 : **E111**	
Light Chain H Bonds	Y54 : **Q154**	Y54 : **T156**
		S61 : **G119**

C

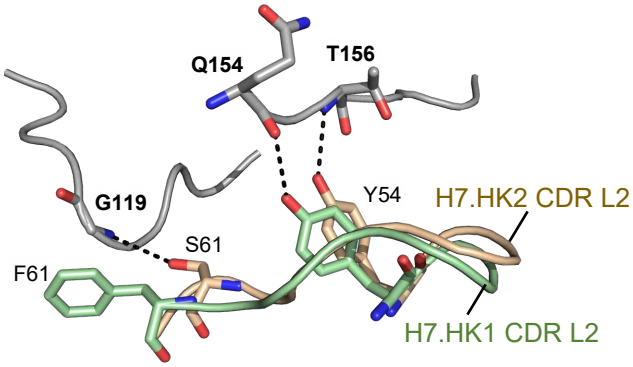

Supplementary Fig. 3 Comparison of H7.HK1 and H7.HK2 binding to H7. (**A**) Differences in epitopes of H7.HK1 and H7.HK2. Majority of surface contacts are conserved, shown in orange. H7.HK1 specific surfaces are shown in magenta, and H7.HK2 specific surfaces are shown in cyan. (**B**) Hydrogen bonds and salt bridges formed by H7.HK1 and H7.HK2 with H7. (**C**) Differences in CDR L2 binding to H7 by H7.HK1 and H7.HK2 as a result of F61S substitution in H7.HK2. S61 forms an additional hydrogen bond with G119 of H7. Additionally, position of Y54 is shifted so that it forms a hydrogen bond with T156 for H7.HK2 instead of Q154 for H7.HK1.

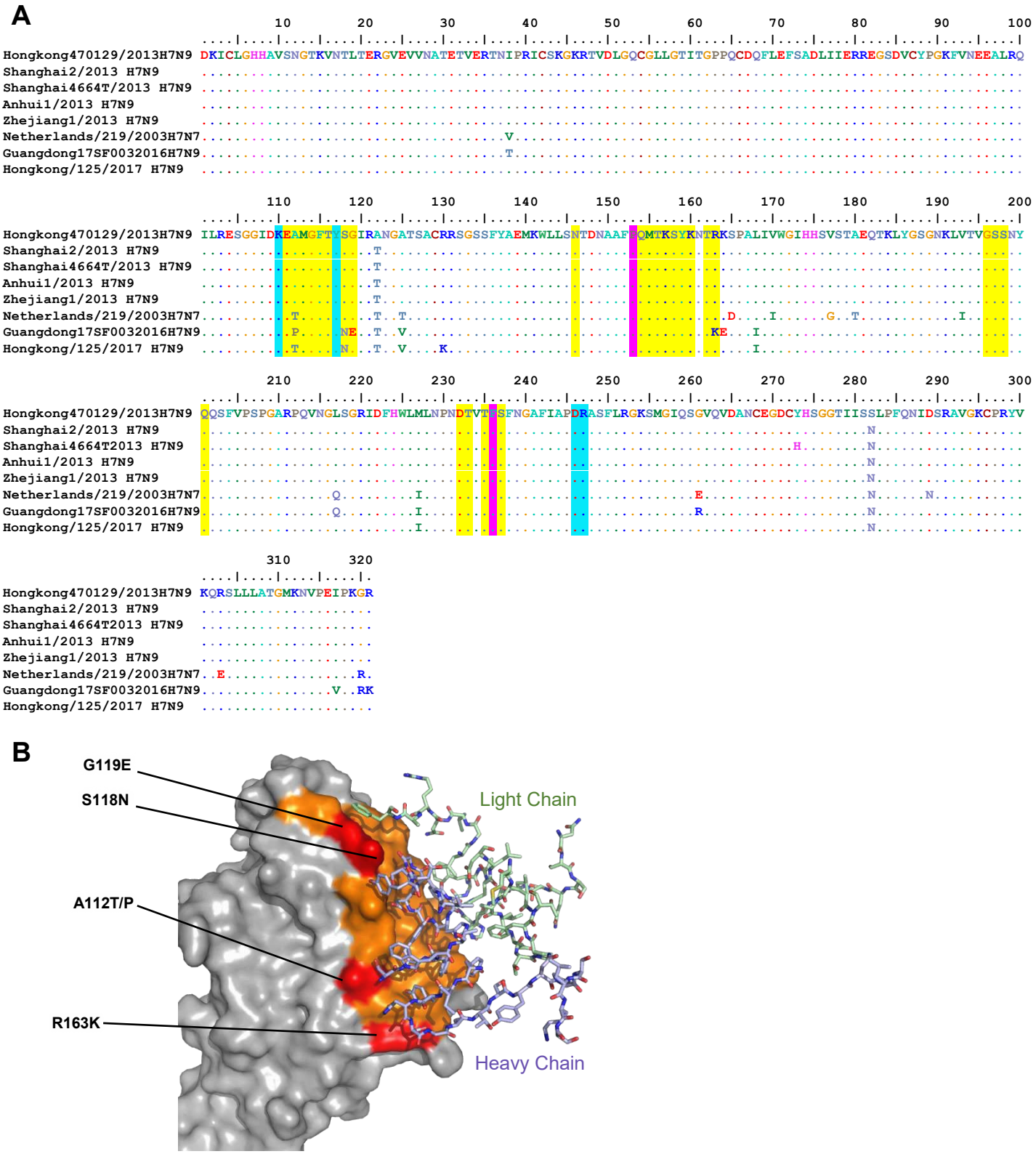

Supplementary Fig. 4 Antigenic drift of H7 HA1 in 2016-2017. (**A**) H7 HA1 protein sequences from the indicated viral isolates are aligned to the 2013 Hong Kong H7N9 autologous isolate at top, with identical amino acids shown in dots. Highlighted in yellow are the H7 residues (epitope) forming contacts with both mAbs H7.HK1 and H7.HK2. H7.HK1 specific epitopes are in magenta; H7.HK2 specific epitopes are in cyan. (**B**) Surface presentation of the H7 HA1 domain highlighting the epitopes (orange) of mAbs H7.HK1 and H7.HK2, with four mutations in red that appeared in the 2016-2017 viral isolates of H7N9. The sticks are interacting CDRs of mAb H7.HK1 heavy and light chains.

Supplementary Table 1 Cryo-EM data collection, refinement, and validation statistics for H7 SH13 DS2 6R HA in complex with H7.HK1 and H7.HK2 Fabs.

	H7 SH13 DS2 6R H7.HK1 (EMD-41422) (PDB: 8TNL)	H7 SH13 DS2 6R H7.HK2 (EMD-41441) (PDB: 8TOA)
Data collection and processing		
Magnification	105000	105000
Voltage (kV)	300	300
Electron exposure (e–/Å^2)	58	58
Defocus range (μm)	0.8-2	0.8-2
Pixel size (Å)	0.83	0.83
Symmetry imposed	C3	C3
Initial particle images (no.)	5713957	2339643
Final particle images (no.)	178347	191469
Map resolution (Å)	3.62	3.69
FSC threshold	0.143	0.143
Refinement		
Initial model used (PDB code)	6IDD	8TNL
Model resolution (Å)	3.62	3.69
FSC threshold	0.143	0.143
Model composition		
Non-hydrogen atoms	16487	15570
Protein residues	2112	2109
Ligands	7	11
B factors (Å^2)		
Protein	39.71	58.34
Ligand	58.78	48.38
R.m.s. deviations		
Bond lengths (Å)	0.005	0.007
Bond angles (°)	1.121	1.231
Validation		
MolProbity score	1.65	2.23
Clashscore	5.45	12.08
Poor rotamers (%)	0.06	1.62
Ramachandran plot		
Favored (%)	94.86	92.30
Allowed (%)	5.14	7.41
Disallowed (%)	0.0	0.29